

Magnetization dynamics and damping due to electron-phonon scattering in a ferrimagnetic exchange model

Alexander Baral,^{1,*} Svenja Vollmar,^{1,2} and Hans Christian Schneider^{1,†}

¹*Physics Department and Research Center OPTIMAS, Kaiserslautern University, P. O. Box 3049, 67663 Kaiserslautern, Germany*

²*Graduate School of Excellence Materials Science in Mainz, Gottlieb-Daimler-Strasse 47, 67663 Kaiserslautern, Germany*

(Received 4 May 2014; revised manuscript received 3 July 2014; published 21 July 2014)

We present a microscopic calculation of magnetization damping for a magnetic “toy model.” The magnetic system consists of itinerant carriers coupled antiferromagnetically to a dispersionless band of localized spins, and the magnetization damping is due to coupling of the itinerant carriers to a phonon bath in the presence of spin-orbit coupling. Using a mean-field approximation for the kinetic exchange model and assuming the spin-orbit coupling to be of the Rashba form, we derive Boltzmann scattering integrals for the distributions and spin coherences in the case of an antiferromagnetic exchange splitting, including a careful analysis of the connection between lifetime broadening and the magnetic gap. For incoherent scattering of itinerant carriers with the phonon bath, i.e., the Elliott-Yafet mechanism, we extract dephasing and magnetization times T_1 and T_2 from initial conditions corresponding to a tilt of the magnetization vector and draw a comparison to phenomenological equations such as the Landau-Lifshitz (LL) or the Gilbert damping. We also analyze magnetization precession and damping for this system including an anisotropy field and find a carrier mediated dephasing of the localized spin via the mean-field coupling.

DOI: [10.1103/PhysRevB.90.014427](https://doi.org/10.1103/PhysRevB.90.014427)

PACS number(s): 75.78.-n, 72.25.Rb, 76.20.+q

I. INTRODUCTION

There are two widely-known phenomenological approaches to describe the damping of a precessing magnetization in an excited ferromagnet: one introduced originally by Landau and Lifshitz [1] and one introduced by Gilbert [2], which are applied to a variety of problems [3] involving the damping of precessing magnetic moments. Magnetization damping contributions and its inverse processes, i.e., spin torques, in particular, in thin films, and nanostructures, are an extremely active field, where currently the focus is on the determination of novel physical processes/mechanisms. Apart from these questions there is still a debate whether the Landau-Lifshitz or the Gilbert damping is the correct one for “intrinsic” damping, i.e., neglecting interlayer coupling, interface contributions, domain structures and/or eddy currents. This intrinsic damping is believed to be caused by a combination of spin-orbit coupling and scattering mechanisms such as exchange scattering between s and d electrons and/or electron-phonon scattering [4–6]. Without reference to the microscopic mechanism, different macroscopic analyses, based, for example, on irreversible thermodynamics or near equilibrium Langevin theory, prefer one or the other description [7,8]. However, the material parameters of typical ferromagnetic heterostructures are such that one is usually firmly in the small damping regime so that several ferromagnetic resonance (FMR) experiments were not able to detect a noticeable difference between Landau-Lifshitz and Gilbert magnetization damping. A recent analysis that related the Gilbert term directly to the spin-orbit interaction arising from the Dirac equation does not seem to have conclusively solved this discussion [9].

The dephasing term in the Landau-Lifshitz form is also used in models based on classical spins coupled to a bath, which have been successfully applied to out-of-equilibrium magnetization dynamics and magnetic switching scenarios [10]. The most fundamental of these are the stochastic Landau-Lifshitz equations [10–13] from which the Landau-Lifshitz Bloch equations [14,15] can be derived via a Fokker-Planck equation.

Quantum-mechanical treatments of the equilibrium magnetization in bulk ferromagnets at finite temperatures are extremely involved. The calculation of nonequilibrium magnetization phenomena and damping for quantum spin systems in more than one dimension, which include both magnetism and carrier-phonon and/or carrier-impurity interactions, at present have to employ simplified models. For instance, there have been microscopic calculations of Gilbert damping parameters based on Kohn-Sham wave functions for metallic ferromagnets [16,17] and Kohn-Luttinger p - d Hamiltonians for magnetic semiconductors [18,19]. While the former approach uses spin density-functional theory, the latter approach treats the antiferromagnetic kinetic-exchange coupling between itinerant p -like holes and localized magnetic moments originating from impurity d electrons within a mean-field theory. In both cases, a constant band (and spin)-independent lifetime for the itinerant carriers is used as an input, and a Gilbert damping constant is extracted by comparing the quantum-mechanical result for $\omega \rightarrow 0$ with the classical formulation. There have also been investigations, which extract the Gilbert damping for magnetic semiconductors from a microscopic calculation of carrier dynamics including Boltzmann-type scattering integrals [20,21]. Such a kinetic approach, which is of a similar type as the one we present in this paper, avoids the introduction of electronic lifetimes because the scattering is calculated dynamically.

The present paper takes up the question how the spin dynamics in the framework of the macroscopic Gilbert or

*baral@rhrk.uni-kl.de

†hcsch@physik.uni-kl.de

Landau-Lifshitz damping compare to a microscopic model of relaxation processes in the framework of a relatively simple model. We analyze a mean-field kinetic exchange model including spin-orbit coupling for the itinerant carriers. Thus the magnetic mean-field dynamics is combined with a microscopic description of damping provided by the electron-phonon coupling. This interaction transfers energy and angular momentum from the itinerant carriers to the lattice. The electron-phonon scattering is responsible both for the lifetimes of the itinerant carriers and the magnetization dephasing. The latter occurs because of spin-orbit coupling in the states that are connected by electron-phonon scattering. To be more specific, we choose an antiferromagnetic coupling at the mean-field level between itinerant electrons and a dispersionless band of localized spins for the magnetic system. To keep the analysis simple, we use as a model for the spin-orbit coupled itinerant carrier states a two-band Rashba model with 2D wave vectors. As such, it is a single-band version of the multiband Hamiltonians used for III-Mn-V ferromagnetic semiconductors [18,22–26]. The model analyzed here also captures some properties of two-sublattice ferrimagnets, which are presently investigated because of their magnetic switching dynamics [27,28]. Our paper is set apart from studies of spin dynamics in similar models with more complicated itinerant band structures [20,21] by a detailed comparison of the phenomenological damping expressions with a microscopic calculation as well as a careful analysis of the restrictions placed by the size of the magnetic gap on the single-particle broadening in Boltzmann scattering integrals.

This paper is organized as follows. As an extended introduction, we review in Sec. II some basic facts concerning the Landau-Lifshitz and Gilbert damping terms on the one hand and the Bloch equations on the other. In Sec. III, we point out how these different descriptions are related in special cases. We then introduce a microscopic model for the dephasing due to electron-phonon interaction in Sec. IV, and present numerical solutions for two different scenarios in Secs. V and VI. The first scenario is the dephasing between two spin subsystems (Sec. V), and the second scenario is a relaxation process of the magnetization toward an easy axis (Sec. VI). A brief conclusion is given at the end.

II. PHENOMENOLOGIC DESCRIPTIONS OF DEPHASING AND RELAXATION

We summarize here some results pertaining to a single-domain ferromagnet and set up our notation. In equilibrium, we assume the magnetization to be oriented along its easy axis or a magnetic field \vec{H} , which we take to be the z axis in the following. If the magnetization is tilted out of equilibrium, it starts to precess. As illustrated in Fig. 1, one distinguishes the longitudinal component M_{\parallel} , in z direction, and the transverse part $M_{\perp} \equiv \sqrt{M^2 - M_{\parallel}^2}$, precessing in the x - y plane with the Larmor frequency ω_L .

In connection with the interaction processes that return the system to equilibrium, the decay of the transverse component is called dephasing. There are three phenomenological equations used to describe spin dephasing processes: (1) the Bloch

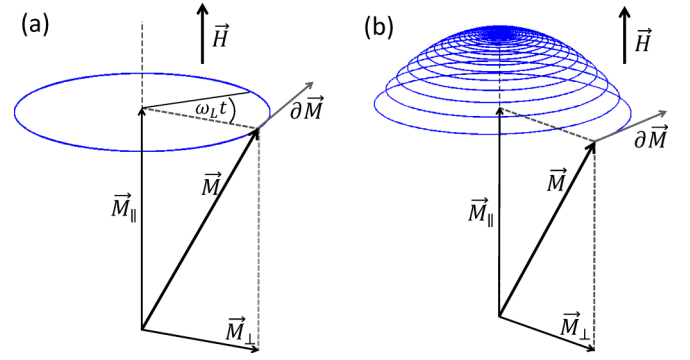


FIG. 1. (Color online) Illustration of nonequilibrium spin dynamics in presence of a magnetic field without relaxation (a) and within relaxation (b).

(-Bloembergen) equations [29,30]

$$\frac{\partial}{\partial t} M_{\parallel}(t) = -\frac{M_{\parallel}(t) - M^{\text{eq}}}{T_1}, \quad (1)$$

$$\frac{\partial}{\partial t} M_{\perp}(t) = -\frac{M_{\perp}(t)}{T_2} \quad (2)$$

describe an exponential decay towards the equilibrium magnetization M^{eq} in z direction. The transverse component decays with a time constant T_2 , whereas the longitudinal component approaches its equilibrium amplitude with T_1 . These time constants may be fit independently to experimental results or microscopic calculations.

(2) Landau-Lifshitz damping [1] with parameter λ ,

$$\frac{\partial}{\partial t} \vec{M}(t) = -\gamma \vec{M} \times \vec{H} - \lambda \frac{\vec{M}}{M} \times (\vec{M} \times \vec{H}), \quad (3)$$

where γ is the gyromagnetic ratio. The first term models the precession with a frequency $\omega_L = \gamma |\vec{H}|$, whereas the second term is solely responsible for damping.

(3) Gilbert damping [2] with the dimensionless Gilbert damping parameter α :

$$\frac{\partial}{\partial t} \vec{M}(t) = -\gamma_G \vec{M} \times \vec{H} + \alpha \left(\frac{\vec{M}}{M} \times \partial_t \vec{M} \right). \quad (4)$$

It is generally accepted that α is independent of the static magnetic fields \vec{H} such as anisotropy fields [18,31], and thus depends only on the material and the microscopic interaction processes.

The Landau-Lifshitz and Gilbert forms of damping are mathematically equivalent [2,7,32] with

$$\alpha = \frac{\lambda}{\gamma}, \quad (5)$$

$$\gamma_G = \gamma(1 + \alpha^2), \quad (6)$$

but there are important differences. In particular, an increase of α lowers the precession frequency in the dynamics with Gilbert damping, while the damping parameter λ in the Landau-Lifshitz equation has no impact on the precession. In contrast to the Bloch equations, Landau-Lifshitz and Gilbert spin dynamics always conserve the length $|\vec{M}|$ of the magnetization vector.

An argument by Pines and Slichter [33] shows that there are two different regimes for Bloch-type spin dynamics depending on the relation between the Larmor period and a “correlation time.” The correlation time as used by Pines and Slichter is the typical time scale over which the precession frequency is largely unchanged by interactions with an environment. As long as this correlation time is much longer than the Larmor period, the system “knows” the direction of the field during the scattering process. Stated differently, the scattering process “sees” the magnetic gap in the band structure. Thus the transverse and longitudinal spin components are distinguishable and the Bloch decay times T_1 and T_2 can differ. If the correlation time is considerably shorter than the Larmor period, this distinction is not possible, with the consequence that T_1 must be equal to T_2 . Within the microscopic approach, presented in Sec. IV D, this consideration shows up again, albeit for the energy conserving δ functions resulting from a Markov approximation.

The regime of short correlation times has already been investigated in the framework of a microscopic calculation by Wu and coworkers [34]. They analyze the case of a moderate external magnetic field applied to a nonmagnetic n -type GaAs quantum well and include different scattering mechanisms (electron-electron Coulomb, electron-phonon, electron impurity). They argue that the momentum relaxation rate is the crucial time scale in this scenario, which turns out to be much larger than the Larmor frequency. Their numerical results confirm the identity $T_1 = T_2$ expected from the Pines-Slichter argument.

III. RELATION BETWEEN LANDAU-LIFSHITZ, GILBERT, AND BLOCH

We highlight here a connection between the Bloch equations (1) and (2) and the Landau-Lifshitz equation (3). To this end, we assume a small initial tilt of the magnetization and describe the subsequent dynamics of the magnetization in the form

$$\vec{M}(t) = \begin{pmatrix} \delta M_{\perp}(t) \cos(\omega_L t) \\ \delta M_{\perp}(t) \sin(\omega_L t) \\ M^{\text{eq}} - \delta M_{\parallel}(t) \end{pmatrix}, \quad (7)$$

where δM_{\perp} and δM_{\parallel} describe deviations from equilibrium. Putting this into Eq. (3), one gets a coupled set of equations:

$$\frac{\partial}{\partial t} \delta M_{\perp}(t) = -\lambda H \frac{M^{\text{eq}} - \delta M_{\parallel}(t)}{|\vec{M}(t)|} \delta M_{\perp}(t), \quad (8)$$

$$\frac{\partial}{\partial t} \delta M_{\parallel}(t) = -\lambda H \frac{1}{|\vec{M}(t)|} \delta M_{\perp}^2(t). \quad (9)$$

Equation (8) is simplified for a small deviation from equilibrium, i.e., $\delta M(t) \ll M^{\text{eq}}$ and $|\vec{M}(t)| \approx M^{\text{eq}}$:

$$\delta M_{\perp}(t) = C \exp(-\lambda H t), \quad (10)$$

$$\delta M_{\parallel}(t) = \frac{C^2}{2M^{\text{eq}}} \exp(-2\lambda H t), \quad (11)$$

where C is an integration constant. For small excitations, the deviations decay exponentially and Bloch decay times T_1 and

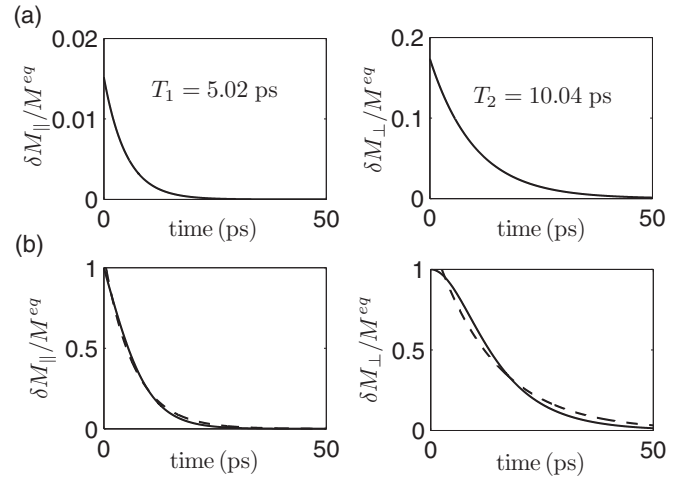


FIG. 2. Dynamics of δM_{\perp} and δM_{\parallel} computed using the Landau-Lifshitz damping ($\omega_L = 1$ ps $^{-1}$, $H = 10^6 \frac{\text{\AA}}{\text{m}} \approx 1.26 \times 10^4$ Oe, and $\lambda = 10^{-7} \frac{\text{m}}{\text{\AA ps}}$). (a) An angle of 10° leads to an exponential decay with well defined T_1 and T_2 times. (b) For an angle of 90° , the decay (solid line) is not exponential as a comparison with the exponential fit (dashed line) clearly shows.

T_2 result, which are related by

$$2T_1 = T_2 = \frac{1}{\lambda H}. \quad (12)$$

Only this ratio of the Bloch times is compatible with a constant length of the magnetization vector at low excitations. By combining Eqs. (12) and (5), one can connect the Gilbert parameter α and the dephasing time T_2 :

$$\alpha = \frac{1}{T_2 \omega_L}. \quad (13)$$

This result will be important in the following, but it is not new, see, e.g., Ref. [35] or the review [36]. We have presented its derivation here, because it is rarely mentioned anymore when magnetic damping phenomena are discussed. If the conditions for the above approximations apply, the Gilbert damping parameter α can be determined by fitting the dephasing time T_2 and the Larmor frequency ω_L to computed or measured spin dynamics. This dimensionless quantity is well suited to compare the dephasing that results from different relaxation processes.

Figure 2 shows the typical magnetization dynamics that results from (3), i.e., Landau-Lifshitz damping. As an illustration of a small excitation, we choose in Fig. 2(a) an angle of 10° for the initial tilt of the magnetization, which results in an exponential decay with $2T_1 = T_2$. From the form of Eq. (3), it is clear that this behavior persists even for large ω_L and λ . Obviously, the Landau-Lifshitz and Gilbert damping terms describe a scenario with relatively long correlation times (i.e., small scattering rates), because only in this regime both decay times can differ. The microscopic formalism in Sec. IV works in the same regime and will be compared with the phenomenological results. For an excitation angle of 90° , the Landau-Lifshitz dynamics shown in Fig. 2(b) becomes nonexponential, so that no well-defined Bloch decay times T_1 and T_2 exist.

IV. MICROSCOPIC MODEL

In this section, we describe a microscopic model that includes magnetism at the mean-field level, spin-orbit coupling as well as the microscopic coupling to a phonon bath treated at the level of Boltzmann scattering integrals. We then compare the microscopic dynamics to the Bloch equations (1) and (2), as well as the Landau-Lifshitz (3) and Gilbert damping terms (4). The magnetic properties of the model are defined by an antiferromagnetic coupling between localized magnetic impurities and itinerant carriers. As a prototypical spin-orbit coupling, we consider an effectively two-dimensional model with a Rashba spin-orbit coupling. The reason for the choice of a model with a two-dimensional wave vector space is not an investigation of magnetization dynamics with reduced dimensionality, but rather a reduction in the dimension of the integrals that have to be solved numerically in the Boltzmann scattering terms. Since we treat the exchange between the localized and itinerant states in a mean-field approximation, our two-dimensional model still has a “magnetic ground state” and presents a framework, for which qualitatively different approaches can be compared. We do not aim at quantitative predictions for, say, magnetic semiconductors or ferrimagnets with two sublattices. Finally, we include a standard interaction Hamiltonian between the itinerant carriers and acoustic phonons. The corresponding Hamiltonian reads

$$\hat{\mathcal{H}} = \hat{\mathcal{H}}_{\text{mf}} + \hat{\mathcal{H}}_{\text{so}} + \hat{\mathcal{H}}_{\text{e-ph}} + \hat{\mathcal{H}}_{\text{aniso}}. \quad (14)$$

Only in Sec. VI an additional field $\hat{\mathcal{H}}_{\text{aniso}}$ is included, which is intended to model a small anisotropy.

A. Exchange interaction between itinerant carriers and localized spins

The “magnetic part” of the model is described by the Hamiltonian

$$\hat{\mathcal{H}}_{\text{mf}} = \sum_{\vec{k}, \mu} \frac{\hbar^2 k^2}{2m^*} \hat{c}_{\vec{k}, \mu}^\dagger \hat{c}_{\vec{k}, \mu} + J \hat{s} \cdot \hat{S}, \quad (15)$$

which we use in the mean-field approximation. The first term represents itinerant carriers with a k -dependent dispersion. In the following, we assume s -like wave functions and parabolic energy dispersions. The effective mass is chosen to be $m^* = 0.5 m_e$, where m_e is the free-electron mass, and the $\hat{c}_{\vec{k}, \mu}^{(\dagger)}$ operators create and annihilate carriers in the state $|\vec{k}, \mu\rangle$, where μ labels the itinerant bands, as shown in Fig. 3(a).

The second term describes the coupling between itinerant spins \vec{s} and localized spins \vec{S} via an antiferromagnetic exchange interaction,

$$\hat{s} = \frac{1}{2} \sum_{\vec{k}} \sum_{\mu, \mu'} \langle \vec{k}, \mu' | \hat{\sigma} | \vec{k}, \mu \rangle \hat{c}_{\vec{k}, \mu}^\dagger \hat{c}_{\vec{k}, \mu'}, \quad (16)$$

$$\hat{S} = \frac{1}{2} \sum_{\nu, \nu'} \langle \nu' | \hat{\sigma} | \nu \rangle \sum_{\vec{K}} \hat{C}_{\vec{K}, \nu}^\dagger \hat{C}_{\vec{K}, \nu'}. \quad (17)$$

Here, we have assumed that the wave functions of the localized spins form dispersionless bands, i.e., we have implicitly

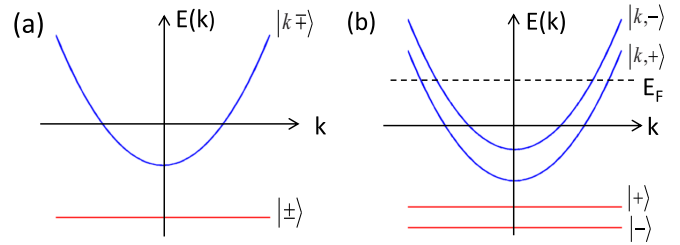


FIG. 3. (Color online) Sketch of the band structure with localized (flat dispersions) and itinerant (parabolic dispersions) electrons. Above the Curie temperature T_C , the spin eigenstates are degenerate (a), whereas below T_C a gap between the spin states exists.

introduced a virtual-crystal approximation. Due to the assumption of strong localization, there is no orbital overlap between these electrons, which are therefore considered to have momentum independent eigenstates $|\nu\rangle$ and a flat dispersion, as illustrated in Fig. 3(a). The components of the vector $\hat{\sigma}$ are the Pauli matrices $\hat{\sigma}_i$ with $i = x, y, z$, and $\hat{C}_{\vec{K}, \nu}^{(\dagger)}$ are the creation and annihilation operators for a localized spin state.

The virtual crystal approximation already excludes a direct interaction among the localized spins and we do not include any interactions among itinerant carriers either. For simplicity, we assume both itinerant and localized electrons to have a spin 1/2 and therefore μ and ν to run over two spin-projection quantum numbers $\pm 1/2$. In the following numerical calculation, we choose an antiferromagnetic ($J > 0$) exchange constant $J = 500$ meV, which leads to the schematic band structure shown in Fig. 3(b). Apart from a different sign in the spin expectation value of one subsystem, a ferromagnetic coupling constant would yield the same results and the statements of this paper should qualitatively still be valid.

In the mean-field approximation used here, the itinerant carriers feel an effective magnetic field \vec{H}_{loc} ,

$$\vec{H}_{\text{loc}} = -\frac{J \mu_B \mu}{g} \vec{S}, \quad (18)$$

caused by localized moments and vice versa. Here, μ_B is the Bohr magneton and $g = 2$ is the g factor of the electron. The permeability μ is assumed to be the vacuum permeability μ_0 . This time-dependent magnetic field $\vec{H}_{\text{loc}}(t)$ defines the preferred direction in the itinerant subsystem and therefore determines the longitudinal and transverse components of the itinerant spin at each time.

For the exchange interaction between itinerant carriers and localized spins, we stay at the mean-field level. In particular, we do not consider exchange scattering, which in antiferromagnetic systems might lead to fast demagnetization processes. Exchange scattering might also contribute considerably to the dephasing between both sublattices. Since for this kind of dephasing no spin-orbit interaction is necessary, it cannot extract any spin from the system and it is not an Elliott-Yafet like scattering process (see the discussion in Sec. IV D below). Therefore it does not fit into the framework of this paper.

B. Rashba spin-orbit interaction

The Rashba spin-orbit coupling is given by the Hamiltonian

$$\hat{\mathcal{H}}_{\text{so}} = \alpha_{\text{R}}(\hat{\sigma}_x k_y - \hat{\sigma}_y k_x). \quad (19)$$

A Rashba coefficient of $\alpha_{\text{R}} = 10$ meV nm typical for semiconductors is chosen in the following calculations. This value, which is close to the experimental one for the InSb/InAlSb material system [37], is small compared to the exchange interactions, but it allows the exchange of angular momentum with the lattice.

C. Coherent dynamics

From the above contributions (15) and (19) to the Hamiltonian, we derive the equations of motion containing the coherent dynamics due to the exchange interaction and Rashba spin-orbit coupling as well as the incoherent electron-phonon scattering. We first focus on the coherent contributions. In principle, one has the choice to work in a basis with a fixed spin-quantization axis or to use single-particle states that diagonalize the mean-field (plus Rashba) Hamiltonian. Since we intend to use a Boltzmann scattering integral in Sec. IV D we need to apply a Markov approximation, which only works if one deals with diagonalized eigenenergies. In our case, this is the single-particle basis that diagonalizes the entire one-particle contribution of the Hamiltonian $\hat{\mathcal{H}}_{\text{mf}} + \hat{\mathcal{H}}_{\text{so}}$. In matrix representation, this one-particle contribution for the itinerant carriers reads

$$\hat{\mathcal{H}}_{\text{mf}} + \hat{H}_{\text{so}} = \begin{pmatrix} \frac{\hbar^2 k^2}{2m^*} + \Delta_z^{\text{loc}} & (\Delta_+^{\text{loc}} + R_{\vec{k}})^* \\ \Delta_+^{\text{loc}} + R_{\vec{k}} & \frac{\hbar^2 k^2}{2m^*} - \Delta_z^{\text{loc}} \end{pmatrix}, \quad (20)$$

where we have defined $\Delta_i^{\text{loc}} = J \frac{1}{2} \langle \hat{s}_i \rangle$ and $R_{\vec{k}} = -i\alpha_{\text{R}} k \exp(i\varphi_k)$ with $\varphi_k = \arctan(k_y/k_x)$. The eigenenergies are

$$\epsilon_{\vec{k}}^{\pm} = \frac{\hbar^2 k^2}{2m^*} \mp \sqrt{|\Delta_z^{\text{loc}}|^2 + |R_{\vec{k}} + \Delta_+^{\text{loc}}|^2} \quad (21)$$

and the eigenstates

$$|\vec{k}, +\rangle = \begin{pmatrix} 1 \\ \xi_{\vec{k}} \end{pmatrix}; |\vec{k}, -\rangle = \begin{pmatrix} -\xi_{\vec{k}}^* \\ 1 \end{pmatrix}, \quad (22)$$

where

$$\xi_{\vec{k}} = \frac{\Delta_+^{\text{loc}} + R_{\vec{k}}}{\Delta_z^{\text{loc}} + \sqrt{|\Delta_+^{\text{loc}}|^2 + |R_{\vec{k}}|^2}}. \quad (23)$$

In this basis, the coherent part of the equation of motion for the itinerant density matrix $\rho_{\vec{k}}^{\mu\mu'} \equiv \langle \hat{c}_{\vec{k}\mu}^\dagger \hat{c}_{\vec{k}\mu'} \rangle$ reads

$$\frac{\partial}{\partial t} \rho_{\vec{k}}^{\mu\mu'} \Big|_{\text{coh}} = \frac{i}{\hbar} (\epsilon_{\vec{k}}^{\mu} - \epsilon_{\vec{k}}^{\mu'}) \rho_{\vec{k}}^{\mu\mu'}. \quad (24)$$

No mean-field or Rashba terms appear explicitly in these equations of motion since their contributions are now hidden in the time-dependent eigenstates and eigenenergies. Since we are interested in dephasing and precessional dynamics, we assume a comparatively small spin-orbit coupling, that can dissipate angular momentum into the lattice, but does not have a decisive effect on the band structure. Therefore we use the spin mixing only in the transition matrix elements

of the electron-phonon scattering $M_{\vec{k}\mu}^{\vec{k}'\mu'}$ (31). For all other purposes, we set $R_{\vec{k}} = 0$. In particular, the energy-dispersion $\epsilon_{\vec{k}}^{\pm}$ is assumed to be unaffected by the spin-orbit interaction and therefore it is spherically symmetric.

With this approximation, the itinerant eigenstates are always exactly aligned with the effective field of the localized moments $\vec{H}_{\text{loc}}(t)$. Since this effective field changes with time, the diagonalization and a transformation of the spin-density matrix in “spin space” has to be repeated at each time step. This effort makes it easier to identify the longitudinal and transverse spin components with the elements of the single-particle density matrix: the off-diagonal entries of the density matrix $\rho_{\vec{k}}^{\pm\mp}$, which precess with the k -independent Larmor frequency $\omega_{\text{L}} = 2\Delta^{\text{loc}}/\hbar$, always describe the dynamics of the transverse spin component. The longitudinal component, which does not precess, is represented by the diagonal entries $\rho_{\vec{k}}^{\pm\pm}$. Since both components change their spatial orientation continuously, we call this the rotating frame. The components of the spin vector in the rotating frame are

$$\langle \hat{s}_{\parallel} \rangle = \frac{1}{2} \sum_{\vec{k}} (\rho_{\vec{k}}^{++} - \rho_{\vec{k}}^{--}), \quad (25)$$

$$\langle \hat{s}_{\perp} \rangle = \sum_{\vec{k}} |\rho_{\vec{k}}^{\pm\mp}|. \quad (26)$$

The components in the fixed frame are obtained from Eq. (16):

$$\langle \hat{s} \rangle = \frac{1}{2} \sum_{\vec{k}} \sum_{\mu\mu'} \langle \vec{k}, \mu' | \hat{\sigma} | \vec{k}, \mu \rangle \rho_{\vec{k}}^{\mu\mu'}. \quad (27)$$

In this form, the time-dependent states carry the information how the spatial components are described by the density matrix at each time step. No time-independent “longitudinal” and “transverse” directions can be identified in the fixed frame.

In a similar fashion, the diagonalized single-particle states of the localized spin system are obtained. The eigenenergies are

$$E^{\pm} = \mp |\bar{\Delta}^{\text{itin}}|, \quad (28)$$

where $\Delta_i^{\text{itin}} = J \frac{1}{2} \langle \hat{s}_i \rangle$ is the localized energy shift caused by the itinerant spin component s_i . The eigenstates are again always aligned with the itinerant magnetic moment. In this basis, the equation of motion of the localized spin-density matrix $\rho_{\text{loc}}^{vv'} \equiv \sum_{\vec{K}} \langle \hat{C}_{\vec{K}v}^\dagger \hat{C}_{\vec{K}v'} \rangle$ is simply

$$\frac{\partial}{\partial t} \rho_{\text{loc}}^{vv'} = \frac{i}{\hbar} (E^v - E^{v'}) \rho_{\text{loc}}^{vv'} \quad (29)$$

and does not contain explicit exchange contributions. Equations (25)–(27) apply in turn to the components $\langle S_{\parallel} \rangle$ and $\langle S_{\perp} \rangle$ of the localized spin and its spin-density matrix $\rho_{\text{loc}}^{vv'}$.

D. Electron-phonon Boltzmann scattering with spin splitting

Relaxation is introduced into the model by the interaction of the itinerant carriers with a phonon bath, which plays the role of an energy and angular momentum sink for the carriers. Our goal here is to present a derivation of the Boltzmann scattering contributions using standard methods,

see, e.g., Refs. [38,39], and to show that the use of a standard spin-dependent Boltzmann scattering integral is limited by the size of the magnetic gap. As a technical simplification, we keep the spin-mixing due to Rashba spin-orbit interaction only in the scattering integral, but not in the coherent dynamics of the spin-density matrix, as done, e.g., by Shen and Wu [21]. Since spin relaxation due to incoherent scattering processes is often referred to as the Elliott-Yafet mechanism, this approximation means we effectively include only Elliott-Yafet type spin relaxation. The Dyakonov-Perel mechanism [20,34], which essentially works with coherent dynamics due to a spin-orbit induced anisotropic spin splitting, is excluded here. The electron-phonon interaction Hamiltonian reads [38]

$$\hat{H}_{\text{e-ph}} = \sum_{\vec{q}} \hbar \omega_{\vec{q}}^{\text{ph}} \hat{b}_{\vec{q}}^{\dagger} \hat{b}_{\vec{q}} + \sum_{\vec{k}\vec{k}'} \sum_{\mu\mu'} (M_{\vec{k}\mu}^{\vec{k}'\mu'} \hat{c}_{\vec{k}\mu}^{\dagger} \hat{b}_{\vec{k}-\vec{k}'} \hat{c}_{\vec{k}'\mu'} + \text{H.c.}), \quad (30)$$

where $\hat{b}_{\vec{q}}^{(\dagger)}$ are the bosonic operators that create or annihilate acoustic phonons with momentum \vec{q} and linear dispersion $\omega_{\text{ph}}(q) = c_{\text{ph}}|\vec{q}|$. The sound velocity is taken to be $c_{\text{ph}} = 40$ nm/ps and we use an effectively two-dimensional transition matrix element [40]

$$M_{\vec{k}\mu}^{\vec{k}'\mu'} = D \sqrt{|\vec{k} - \vec{k}'|} \langle \vec{k}, \mu | \vec{k}', \mu' \rangle, \quad (31)$$

where the deformation potential is chosen to be $D = 60$ meV nm^{1/2}. The scalar product between the initial state $|\vec{k}', \mu'\rangle$ and the final state $|\vec{k}, \mu\rangle$ of an electronic transition takes the spin mixing due to Rashba spin-orbit coupling into account.

The derivation of Boltzmann scattering integrals for the itinerant spin-density matrix (24) leads to a memory integral of the following shape:

$$\left. \frac{\partial}{\partial t} \rho_j(t) \right|_{\text{inc}} = \frac{1}{\hbar} \sum_{j'} \int_{-\infty}^t e^{i(\Delta E_{jj'} + i\gamma)(t-t')} F_{jj'}[\rho(t')] dt', \quad (32)$$

regardless whether one uses Green's function [39] or equation-of-motion techniques [38]. Since we go through a standard derivation here, we highlight only the important parts for the present case and do not write the equations out completely. In particular, for a scattering process $j' = |\mu', \vec{k}'\rangle \rightarrow j = |\mu, \vec{k}\rangle$, we use $F_{jj'}[\rho(t')]$ as an abbreviation for a product of dynamical electronic spin-density matrix elements ρ , evaluated at time $t' < t$, and equilibrium phononic distributions. The corresponding energy difference is denoted by $\Delta E_{jj'} = E_j - E_{j'} \pm \hbar \omega_{\text{ph}}(|\vec{k} - \vec{k}'|)$, and γ describes the decay of the exponential function due to dissipation and/or higher order correlation functions. In general, the integral has to be evaluated numerically and contains memory effects. To apply the Markov approximation one needs to compare two time scales: the ‘‘memory depth’’ $1/\gamma$, i.e., the time scale on which the $\exp[-\gamma(t - t')]$ factor essentially cuts off the integral, and the typical time scale on which the F term changes. In this paper, we deal with relaxation processes not too far away from equilibrium, so that the typical time scale of the components of

the spin-density matrix contained in F is set by the Bloch times T_1 and T_2 . We can thus approximate $F_{jj'}[\rho(t')]$ by $F_{jj'}[\rho(t)]$, for all transitions labeled by j and j' , if the memory depth is shorter than the Bloch time(s), or

$$\gamma \gg \frac{1}{T_1}. \quad (33)$$

Provided condition (33) holds, the integral (32) can be done using the Markov approximation $F_{jj'}[\rho(t')] \simeq F_{jj'}[\rho(t)]$:

$$\left. \frac{\partial}{\partial t} \rho_j(t) \right|_{\text{incoh}} = \frac{i}{\hbar} \sum_{j'} F_{jj'}[\rho(t)] \frac{1}{\Delta E_{jj'} + i\hbar\gamma}. \quad (34)$$

As it is customary, we neglect in the following the real part of the complex energy denominator, which results in shifts of the single-particle energies. While these shifts may play an important role in non-Markovian problems with discrete energy levels [41], the imaginary parts yield the relaxation contributions that are important for the present paper:

$$\left. \frac{\partial}{\partial t} \rho_j(t) \right|_{\text{incoh}} = \sum_{j'} F_{jj'}[\rho(t)] \frac{\hbar\gamma}{(\Delta E_{jj'})^2 + (\hbar\gamma)^2}. \quad (35)$$

All transitions are thus weighted by a Lorentzian peaked at resonant transitions ($\Delta E_{jj'} = 0$) with a broadening of $\hbar\gamma$ that may be interpreted as an energy uncertainty. For relaxation processes in a system with a spin splitting (due to internal fields and/or spin-orbit coupling), this broadening must not be so large as to blur the distinction between the split bands. Consequently, only if the broadening γ is smaller than the magnetic splitting, i.e., if $\gamma \ll \omega_L$, it is possible to distinguish between longitudinal and transverse components of the spin-density matrix. With Eq. (33) the inequality $\gamma \ll \omega_L$ yields the condition

$$\omega_L \gg \frac{1}{T_1} \quad (36)$$

for the Larmor frequencies and Bloch times, for which it is permissible to replace the Lorentzian by an energy conserving δ function

$$\frac{\hbar\gamma}{(\Delta E_{jj'})^2 + (\hbar\gamma)^2} \xrightarrow{\gamma \rightarrow 0} \pi \delta(\Delta E_{jj'}). \quad (37)$$

This reduces the numerical effort very considerably because it allows one to eliminate an integration from the scattering term.

The considerations leading to the connection between Eqs. (36) and (37) are a microscopic version of an argument due to Pines and Slichter [33], according to which T_1 and T_2 can differ only for correlation times that are long in comparison to a Larmor period. The microscopic Boltzmann scattering terms, which contain the energy conserving δ functions and will be used in the following, do not apply in a regime outside of condition (36). If $\omega_L \simeq 1/T_1$, the Markov approximation becomes questionable. We thus obtain the full equation of motion

for the itinerant-carrier spin density matrix in the regime (36):

$$\begin{aligned}
\frac{\partial}{\partial t} \rho_{\vec{k}}^{\mu\mu'} &= \frac{i}{\hbar} (\epsilon_{\vec{k}}^{\mu} - \epsilon_{\vec{k}}^{\mu'}) \rho_{\vec{k}}^{\mu\mu'} \\
&+ \frac{\pi}{\hbar} \sum_{\vec{k}'} \sum_{\mu_1\mu_2\mu_3} M_{\vec{k}'\mu_1}^{\vec{k}\mu} M_{\vec{k}\mu_3}^{\vec{k}'\mu_2} \delta(\Delta E_{\vec{k}'\mu_2\vec{k}\mu_3}) \left[\left(1 + N_{|\vec{k}'-\vec{k}|}^{\text{ph}}\right) \rho_{\vec{k}'}^{\mu_1\mu_2} (\delta_{\mu_3\mu'} - \rho_{\vec{k}}^{\mu_3\mu'}) - N_{|\vec{k}'-\vec{k}|}^{\text{ph}} \rho_{\vec{k}}^{\mu_3\mu'} (\delta_{\mu_1\mu_2} - \rho_{\vec{k}'}^{\mu_1\mu_2}) \right] \\
&- \frac{\pi}{\hbar} \sum_{\vec{k}'} \sum_{\mu_1\mu_2\mu_3} M_{\vec{k}'\mu_1}^{\vec{k}\mu} M_{\vec{k}\mu_3}^{\vec{k}'\mu_2} \delta(\Delta E_{\vec{k}\mu_3\vec{k}'\mu_2}) \left[\left(1 + N_{|\vec{k}-\vec{k}'|}^{\text{ph}}\right) \rho_{\vec{k}}^{\mu_3\mu_1} (\delta_{\mu_1\mu_2} - \rho_{\vec{k}'}^{\mu_1\mu_2}) - N_{|\vec{k}-\vec{k}'|}^{\text{ph}} \rho_{\vec{k}'}^{\mu_1\mu_2} (\delta_{\mu_3\mu'} - \rho_{\vec{k}}^{\mu_3\mu'}) \right] \\
&+ \frac{\pi}{\hbar} \sum_{\vec{k}'} \sum_{\mu_1\mu_2\mu_3} M_{\vec{k}'\mu_1}^{\vec{k}\mu} M_{\vec{k}\mu_2}^{\vec{k}'\mu_3} \delta(\Delta E_{\vec{k}'\mu_2\vec{k}\mu_3}) \left[\left(1 + N_{|\vec{k}'-\vec{k}|}^{\text{ph}}\right) \rho_{\vec{k}'}^{\mu_2\mu_1} (\delta_{\mu_2\mu_3} - \rho_{\vec{k}}^{\mu_2\mu_3}) - N_{|\vec{k}'-\vec{k}|}^{\text{ph}} \rho_{\vec{k}}^{\mu_2\mu_3} (\delta_{\mu_2\mu_1} - \rho_{\vec{k}'}^{\mu_2\mu_1}) \right] \\
&- \frac{\pi}{\hbar} \sum_{\vec{k}'} \sum_{\mu_1\mu_2\mu_3} M_{\vec{k}'\mu_1}^{\vec{k}\mu} M_{\vec{k}\mu_2}^{\vec{k}'\mu_3} \delta(\Delta E_{\vec{k}\mu_3\vec{k}'\mu_2}) \left[\left(1 + N_{|\vec{k}-\vec{k}'|}^{\text{ph}}\right) \rho_{\vec{k}}^{\mu_3\mu_1} (\delta_{\mu_2\mu_1} - \rho_{\vec{k}'}^{\mu_2\mu_1}) - N_{|\vec{k}-\vec{k}'|}^{\text{ph}} \rho_{\vec{k}'}^{\mu_2\mu_1} (\delta_{\mu_3\mu_3} - \rho_{\vec{k}}^{\mu_3\mu_3}) \right].
\end{aligned} \tag{38}$$

Here, $\Delta E_{\vec{k}\mu\vec{k}'\mu'} = \epsilon_{\vec{k}}^{\mu} - \epsilon_{\vec{k}'}^{\mu'} - \hbar\omega_{|\vec{k}-\vec{k}'|}^{\text{ph}}$ and N_q^{ph} is the occupation function of a thermalized phonon bath, given by a Bose-Einstein distribution:

$$N_q^{\text{ph}} = \frac{1}{e^{\beta\hbar\omega_{\text{ph}}} - 1}, \tag{39}$$

where $\beta = 1/(k_{\text{B}}T_{\text{ph}})$. The numerical results for the microscopic dynamics in the following sections are obtained by numerically solving the equations of motion (29) and (38). In the numerical calculations, the spin-density matrix is transformed to the single-particle basis of the instantaneous, diagonalized eigenstates (22).

V. DEPHASING BETWEEN LOCALIZED AND ITINERANT SPINS: NUMERICAL RESULTS

Since we are interested in this paper in a comparison of the model described above with Landau-Lifshitz and Gilbert damping, we investigate magnetization dynamics with an initial spin-density matrix that corresponds to a tilting of the spins out of their equilibrium position *without* changing the kinetic energy of the carriers, because we need initial conditions that lead to generic magnetization dephasing without carrier heating and the corresponding demagnetization dynamics.

A. Initial state and spin dynamics

Thus we take as the equilibrium initial state the steady state that is reached for the coupled spins interacting with the phonon bath at a low temperature of $T_{\text{ph}} = 1$ K, as shown in Fig. 4(a). The chosen temperature has only a negligible impact

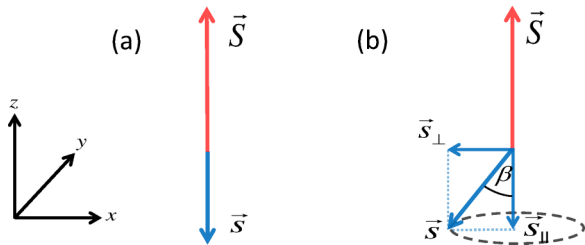


FIG. 4. (Color online) (a) Localized spin $\langle \vec{S} \rangle$ and itinerant spin $\langle \vec{S} \rangle$ in thermal equilibrium. (b) Itinerant spin tilted relatively to the localized spin by an angle β .

on the resulting dynamics as long as it is small compared to the Curie temperature T_C , which avoids heat-induced demagnetization dynamics. In this equilibrium state, the spin density matrix is characterized by shifted Fermi functions for the distributions $\rho_{\vec{k}}^{\mu\mu} = f(\epsilon_{\vec{k}}^{\mu} - E_{\text{F}}, T_{\text{ph}})$ and vanishing coherences $\rho_{\vec{k}}^{\pm\mp} = 0$. Due to the dispersion of the carriers, in equilibrium, the itinerant spin \vec{s} is shorter than the localized spin \vec{S} , which is completely polarized.

We then change the itinerant density matrix to that corresponding to an itinerant spin tilted by $\beta = 10^\circ$ relative to its equilibrium orientation determined by the localized spin, see Fig. 4(b). This initial condition achieves a tilting of the spins without heating and avoids generic de- and remagnetization dynamics. Microscopically, the tilted spin corresponds to the spin density matrix shown in Fig. 5. The perturbation for distributions and coherences exists only between the two Fermi wave vectors for the $\mu = +$ and $\mu = -$ bands. For smaller tilt angles, the deviation is much less pronounced.

From this initial condition, both spins start to precess around the instantaneous direction, along which the exchange interaction tries to align them. This direction is determined for the itinerant carriers by the localized spins and vice versa. The precession frequencies of both spins are different, because of the different polarizations. A return back into equilibrium requires the scattering of itinerant electrons with phonons. If

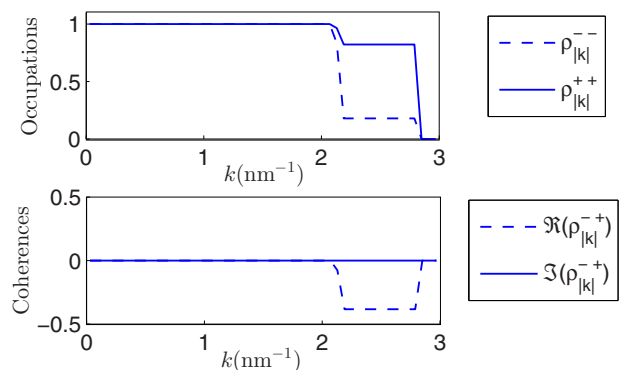


FIG. 5. (Color online) Initial spin density-matrix (occupations and coherences) for itinerant electrons corresponding to a relative tilt $\beta = 50^\circ$. The deviation from equilibrium occurs only between the Fermi wave vectors of the “+” and “-” bands.

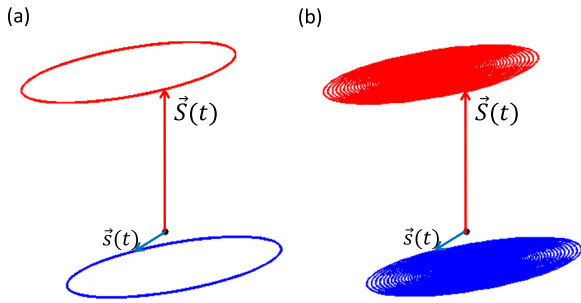


FIG. 6. (Color online) Nonequilibrium dynamics of localized (red) and itinerant (blue) spins including electron-phonon scattering without (a) and with (b) spin mixing.

we switch off spin mixing, the dynamics shown in Fig. 6(a) results: no angular momentum is exchanged with the phonon bath, the excited system cannot relax into equilibrium, and the precession goes on indefinitely. Figure 6(b) shows the same result including spin-mixed itinerant states. Now, angular momentum can be transferred from the itinerant subsystem into the lattice and the total spin $\vec{S} + \vec{s}$ changes. In the presence of spin-orbit coupling, electron-phonon scattering, which is by itself spin-diagonal, can return the spin system into equilibrium, characterized by aligned spins and vanishing transverse components. Since we consider here a small Rashba coupling, the interaction with the phonon bath removes energy much faster than angular momentum. The carrier temperature therefore stays practically equal to the phonon temperature T_{ph} during the entire relaxation process, and no heat-induced demagnetization processes occur. The final magnetization is, however, not necessarily oriented in the z direction of the fixed frame, because in the results discussed in this section there is no external field or anisotropy to induce such an alignment.

We plot the resulting dynamics of the itinerant spins during the dephasing process in Fig. 7, which shows that all itinerant spatial components precess, and no spatially fixed component can be considered to be longitudinal. First, the localized spin turns away from the z direction due to the tilted itinerant spin and subsequently both spin systems precess around each other because the quantization axis of each system changes continuously due to the mutual interaction. During the entire relaxation process the absolute value of the itinerant spin is conserved to better than 1%. Figure 8 shows the same dynamics in the rotating frame, where the longitudinal and transverse dynamics can be seen clearly. Both itinerant components show exponential dynamics, which are therefore well described by decay times T_1 and T_2 . If well-defined decay times exist, one expects a ratio $T_2/T_1 = 2$ as long as the length of the spin is conserved. The fit for our numerical results indeed gives $2T_1 \simeq T_2$.

Figure 9 plots the T_1 and T_2 values extracted from the dynamics as a function of the strength of the electron-phonon coupling, or deformation potential D . The dependence of the decay times on D can be fit extremely well by a $1/D^2$ relation, which demonstrates the proportionality of the Bloch decay times $T_{1,2} \propto 1/D^2$. Further, the ratio T_2/T_1 stays equal to 2 for all coupling strengths. As discussed in Sec. IV D about the Markov approximation, our microscopic description cannot reach regimes where T_1 and T_2 are indistinguishable

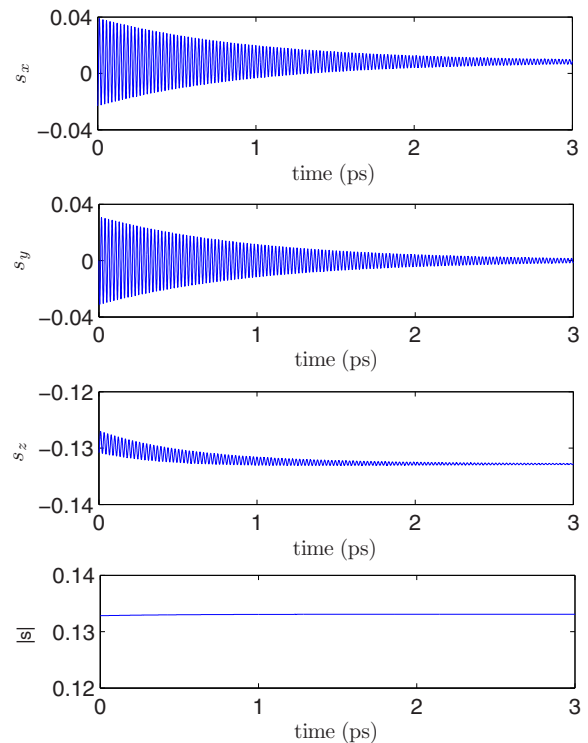


FIG. 7. (Color online) Relaxation dynamics of itinerant spins in the fixed frame.

and therefore equal. However, these results show that for small tilting angles, not even a pronounced electron-phonon coupling leads to a noticeable deviation from the $T_2 = 2T_1$ behavior. Because this relation between T_1 and T_2 holds, the dynamics in Fig. 8 can be equally well described by a Landau-Lifshitz or Gilbert damping terms. By fitting the dephasing time $T_2 \approx 1$ ps and the Larmor frequency $\omega_L \approx 281 \text{ ps}^{-1}$ of the itinerant spin, Eq. (13) yields the corresponding itinerant Gilbert damping parameter $\alpha_{\text{iso}} \approx 3.6 \times 10^{-3}$. In Ref. [21], Shen and Wu extracted a Gilbert parameter from a microscopic calculation of hole-spin dynamics in a bulk magnetic semiconductor. Due to a larger phase space and a stronger spin-orbit coupling, they find a value of about $\alpha \approx 0.05$, i.e., one order of magnitude larger than ours.

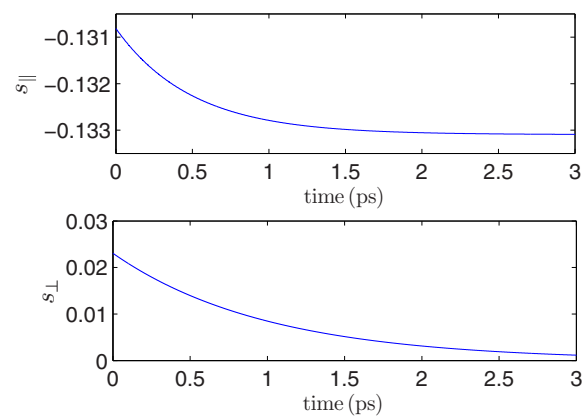


FIG. 8. (Color online) Relaxation dynamics of itinerant spins in the rotating frame. An exponential fit determines the Bloch decay times to $T_1 = 0.5$ ps and $T_2 = 1.0$ ps.

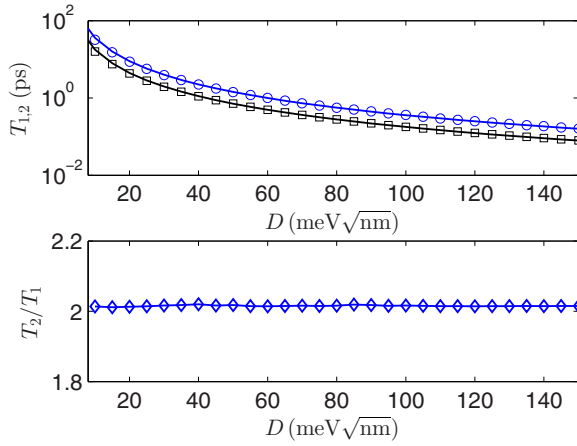


FIG. 9. (Color online) (Top) Longitudinal (black squares) and transverse (blue circles) Bloch decay times vs electron-phonon coupling strength D together with two fit curves $\propto 1/D^2$ (solid lines). To a good approximation $T_{1,2} \propto 1/D^2$. (Bottom) Ratio T_2/T_1 of both decay times vs coupling strength.

B. Precession-frequency shift due to dephasing

In the Landau-Lifshitz equation, the contributions describing, respectively, the precession and the damping are completely independent, so that the damping constant λ has no impact on the precession. By contrast, an increase of α in the Gilbert equation does not only increase the dephasing rate, it lowers the precession frequency as well.

In this section, we investigate the change of the precession frequency of the itinerant spin in the microscopic calculation and compare it with the macroscopic descriptions. To this end, we use the off-diagonal components of the itinerant density matrix $\rho^{+-}(t) = \sum_{\vec{k}} \rho_{\vec{k}}^{+-}(t)$, which describe the dynamics of the transverse spin components in the rotating frame. The modulus of its Fourier transform $|\rho^{+-}(\omega)|$ shows a distinct peak, which is exactly at the precession frequency.

To compare the precession frequency for different damping parameters, we use the dependence on T_2 , because all dephasing parameters can be related to T_2 for small excitations. Figure 10 plots the Larmor frequency of the itinerant spin versus the transverse relaxation rate $1/T_2$. The precession parameters of the Landau-Lifshitz and the Gilbert equations are chosen such that the Larmor frequency in the undamped limiting case is equal to that of the microscopic simulation. In order to stay within the bounds set by condition (36), we

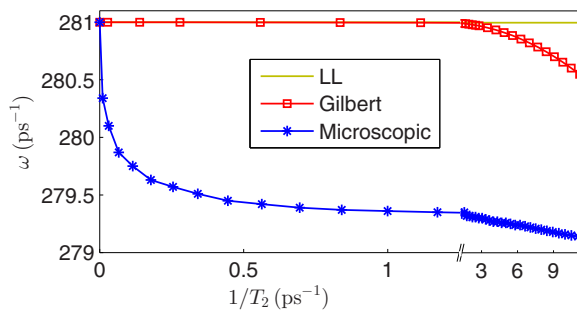


FIG. 10. (Color online) Precession frequency with respect to the damping strength in terms of the decay rate $1/T_2$.

do not extend the plot in Fig. 10 to higher dephasing rates. Figure 10 shows that the microscopic calculation yields a reduction of the precession frequency with the damping rate. Although the Gilbert dynamics also shows such a reduction, it occurs only at shorter T_2 . As mentioned above, for the Landau-Lifshitz damping, the frequency is independent of the damping parameter. Even though the change of precession frequency in the microscopic calculation is small, the Landau-Lifshitz damping completely fails to include this effect. While Gilbert damping does show a reduction of precession frequency, it is not at all close to the microscopic calculation on the frequency scale considered here. Both phenomenological damping expressions thus do not reproduce the dependence of the precession frequency on T_2 . Even though the numerical differences are small, these differences already occur in the small-excitation regime and may perhaps be detectable.

C. Dephasing at larger excitation angles

The phenomenological Landau-Lifshitz and Gilbert damping contributions describe an exponential decay only for small excitation angles, as studied in the previous section. In this section, we investigate the effect of larger excitation angles ($>10^\circ$) on the spin dynamics in the microscopic calculation. Apart from this, the initial condition of the dynamics is the same as before, in particular, the itinerant spin is tilted such that the absolute value of the spin is unchanged.

Figure 11 shows the time development of the s_{\parallel} and s_{\perp} components of the itinerant spin in the rotating frame for an initial tilt angle $\beta = 140^\circ$. While the transverse component s_{\perp} in the rotating frame can be well described by an exponential decay, the longitudinal component s_{\parallel} shows a different behavior. It initially decreases with a time constant of less than 1 ps, but does not reach its equilibrium value. Instead, the eventual return to equilibrium takes place on a much longer timescale, during which the s_{\perp} component is already vanishingly small. The long-time dynamics is therefore purely collinear. For the short-time dynamics, the transverse component can be fit well

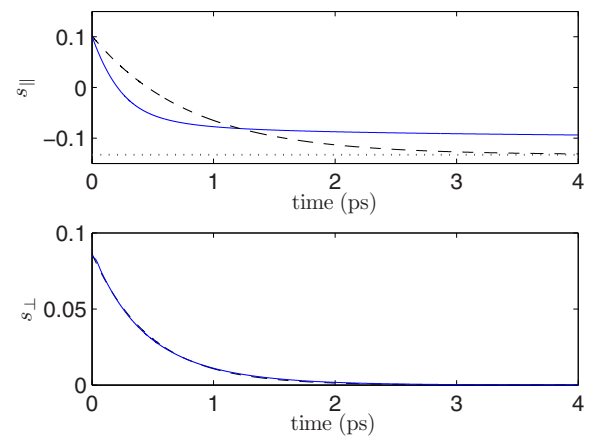


FIG. 11. (Color online) Dynamics of the longitudinal and transverse itinerant spin components in the rotating frame (solid lines) for a tilt angle of $\beta = 140^\circ$, together with exponential fits toward equilibrium (dashed lines). The longitudinal equilibrium polarization is shown as a dotted line. For s_{\perp} , the fit cannot be distinguished from dynamics on this scale.

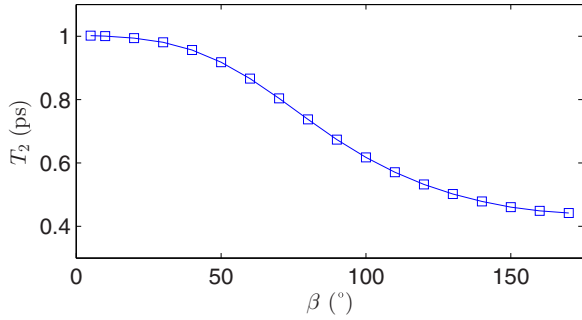


FIG. 12. (Color online) T_2 time extracted from an exponential fit to s_{\perp} dynamics in rotating frame for different initial tilting angles β .

by an exponential decay, even for large excitation angles. This behavior is different from Landau-Lifshitz and Gilbert dynamics, cf. Fig. 2, which both exhibit nonexponential decay of the transverse spin component.

In Fig. 12, the dependence of T_2 on the excitation angle is shown. From small β up to almost 180° , the decay time decreases by more than 50%. This dependence is exclusively due to the “excitation condition,” which involves only spin degrees of freedom (“tilt angle”), but no change of temperature. Although one can fit such a T_2 time to the transverse decay, the overall behavior with its two stages is, in our view, qualitatively different from the typical Bloch relaxation/dephasing picture.

To highlight the similarities and differences from the Bloch relaxation/dephasing, we plot in Fig. 13 the modulus of the itinerant spin vector $|\vec{s}|$ for four different excitation angles. Over the 2 ps, during which the transverse spin in the rotating frame essentially decays, the modulus of the spin vector undergoes a fast initial decrease and a partial recovery. The initial length of \vec{s} is recovered only over a much larger time scale of several hundred picoseconds (not shown). Thus the dynamics can be seen to differ from a Landau-Lifshitz or Gilbert-like scenario because the spin does not precess toward equilibrium with a constant length. Additionally, they differ from Bloch-like dynamics because there is a combination of the fast and slow dynamics that cannot be described by a single

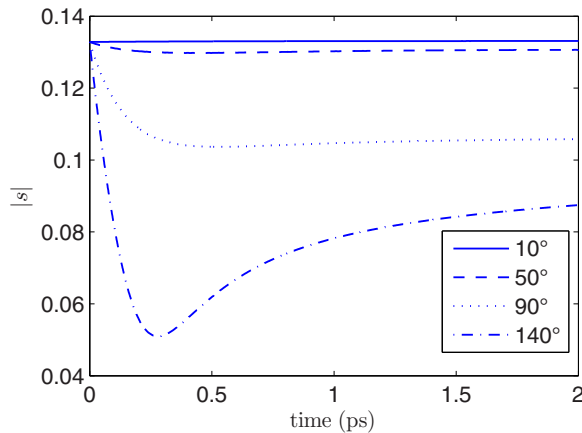


FIG. 13. (Color online) Dynamics of the modulus $|\vec{s}|$ of the itinerant spin for different initial tilt angles β . Note the slightly different time scale compared to Fig. 11.

set of T_1 and T_2 times. We stress that the microscopic dynamics at larger excitation angles shows a precessional motion of the magnetization without heating and a slow remagnetization. This scenario is somewhat in between typical small angle relaxation, for which the modulus of the magnetization is constant and which is well described by Gilbert and Landau-Lifshitz damping, and collinear de/remagnetization dynamics.

The effects that occur after the excitation with a large angle β , i.e., the enhanced T_2 time in Fig. 12 and the reduction of the length of the itinerant spin in Fig. 13, might be detectable in future experiments.

VI. EFFECT OF ANISOTROPY

So far, we have been concerned with the question how phenomenological equations describe dephasing processes between itinerant and localized spins, where the magnetic properties of the system were determined by a mean-field exchange interaction only. Oftentimes, phenomenological models of spin dynamics are used to describe dephasing processes toward an “easy axis” determined by anisotropy fields [31].

In order to capture in a simple fashion the effects of anisotropy on the spin dynamics in our model, we simply assume the existence of an effective anisotropy field \vec{H}_{aniso} , which enters the Hamiltonian via

$$\hat{\mathcal{H}}_{\text{aniso}} = -g\mu_B\mu \hat{s} \cdot \vec{H}_{\text{aniso}} \quad (40)$$

and only acts on the itinerant carriers. Its strength is assumed to be small in comparison to the field of the localized moments \vec{H}_{loc} . This additional field \vec{H}_{aniso} has to be taken into account in the diagonalization of the coherent dynamics as well, see Sec. IV C.

For the investigation of the dynamics with anisotropy, we choose a slightly different initial condition, which is shown in Fig. 14. In thermal equilibrium, both spins are now aligned, with opposite directions, along the anisotropy field \vec{H}_{aniso} , which is assumed to point in the z direction. At $t = 0$, they are both rigidly tilted by an angle $\beta = 10^\circ$ with respect to the anisotropy field.

Figure 14 shows the time evolution of both spins in the fixed frame, with z axis in the direction of the anisotropy field for the same material parameters as in the previous sections and an anisotropy field $\vec{H}_{\text{aniso}} = -10^8 \frac{\text{A}}{\text{m}} \cdot \vec{e}_z$. The dynamics of the entire spin system is somewhat different now, as the itinerant spin precesses around the combined field of the anisotropy and

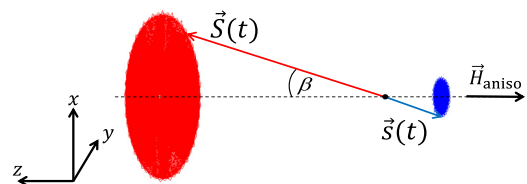


FIG. 14. (Color online) Dynamics of the localized spin \vec{S} and itinerant spin \vec{s} . At $t = 0$, the equilibrium configuration of both spins is tilted ($\beta = 10^\circ$) with respect to an anisotropy field \vec{H}_{aniso} . The anisotropy field is only experienced by the itinerant subsystem.

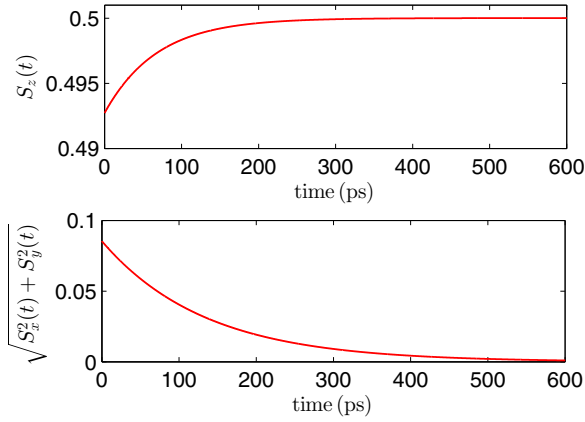


FIG. 15. (Color online) Relaxation dynamics of the localized spin toward the anisotropy direction for longitudinal component S_z and transverse component $\sqrt{S_x^2 + S_y^2}$. An exponential fit yields Bloch decay times of $T_1^{\text{aniso}} = 67.8$ ps and $T_2^{\text{aniso}} = 134.0$ ps.

the localized moments. The localized spin precesses around the itinerant spin, whose direction keeps changing as well.

Figure 15 contains the dynamics of the components of the localized spin in the rotating frame. Both components show an exponential behavior that allows us to extract well defined Bloch-times T_1^{aniso} and T_2^{aniso} . Again, we find the ratio of $2T_1^{\text{aniso}} \approx T_2^{\text{aniso}}$, because the absolute value of the localized spin does not change, as it is not coupled to the phonon bath. Accordingly, the itinerant spin relaxes within the exact same time scale T_1^{aniso} and T_2^{aniso} .

In Fig. 16, the Larmor frequency ω_L^{aniso} , which is the common precession frequency of both the localized and the itinerant spin due to the anisotropy field, and the Bloch decay times T_2^{aniso} are plotted versus the strength of the anisotropy field H_{aniso} . The Gilbert damping parameter α_{aniso} for the dephasing dynamics, which is the same in the localized and

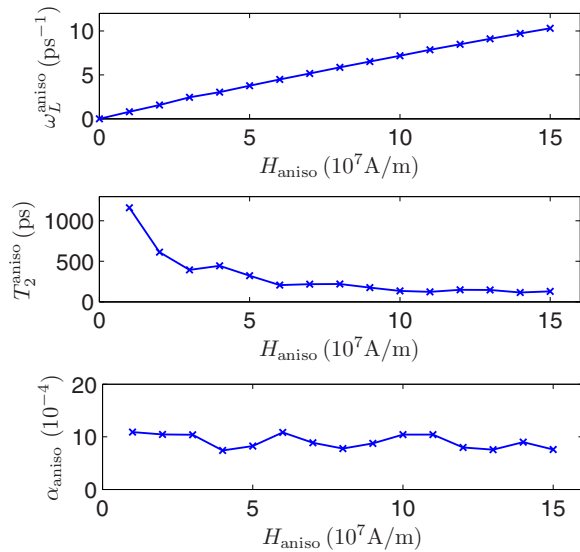


FIG. 16. (Color online) Larmor frequency ω_L^{aniso} and Bloch decay time T_2^{aniso} extracted from the spin dynamics vs anisotropy field H_{aniso} , as well as the corresponding damping parameter α_{aniso} .

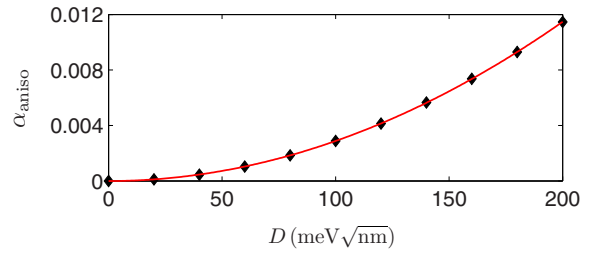


FIG. 17. (Color online) Damping parameter α_{aniso} vs coupling constant D (black diamonds). The red line is a quadratic fit, indicative of $\alpha_{\text{aniso}} \propto D^2$.

the itinerant subsystem, is computed via Eq. (13) and is also presented in this figure.

The plot reveals a decrease of the dephasing time T_2^{aniso} and an almost linear increase of the Larmor frequency ω_L^{aniso} with the strength of the anisotropy field H_{aniso} . The Gilbert damping parameter α_{aniso} shows only a negligible dependence on the anisotropy field H_{aniso} . This confirms the statement that, in contrast to the dephasing rates, the Gilbert damping parameter is independent of the applied magnetic field. In the investigated range, we find an almost constant value of $\alpha_{\text{aniso}} \simeq 9 \times 10^{-4}$.

The Gilbert damping parameter α_{aniso} for the dephasing of both spin systems toward the anisotropy field is about four times smaller than α_{iso} , which describes the dephasing of the itinerant spin toward the field of the localized spin \vec{H}_{loc} . This disparity in the damping efficiency ($\alpha_{\text{aniso}} < \alpha_{\text{iso}}$) is obviously due to a fundamental difference in the dephasing mechanism. In the anisotropy case, the localized spin dephases toward the z direction without being involved in scattering processes with itinerant carriers or phonons. The dynamics of the localized spins is purely precessional due to the time-dependent magnetic moment of the itinerant carriers $\vec{H}_{\text{itin}}(t)$. Thus only this varying magnetic field that turns out to be slightly tilted against the localized spins during the entire relaxation causes the dephasing, in presence of the coupling between itinerant carriers and a phonon bath, which acts as a sink for energy and angular momentum. The relaxation of the localized moments thus occurs only indirectly as a carrier-mediated relaxation via their coupling to the time-dependent mean-field of the itinerant spin.

Next, we investigate the dependence of the Gilbert parameter α_{aniso} on the bath coupling. Figure 17 shows that α_{aniso} increases quadratically with the electron-phonon coupling strength D .

Since Fig. 9 establishes that the spin-dephasing rate $1/T_2$ for the fast dynamics discussed in the previous sections is proportional to D^2 , we find $\alpha_{\text{aniso}} \propto 1/T_2$. We briefly compare these trends to two earlier calculations of Gilbert damping that employ p - d models and assume phenomenological Bloch-type rates $1/T_2$ for the dephasing of the itinerant hole spins toward the field of the localized moments. In contrast to the present paper, the localized spins experience the anisotropy fields. Chovan and Perakis [42] derive a Gilbert equation for the dephasing of the localized spins toward the anisotropy axis, assuming that the hole spin follows the field \vec{H}_{loc} of the localized spins almost adiabatically. Tserkovnyak *et al.* [19] extract a Gilbert parameter from spin susceptibilities. The

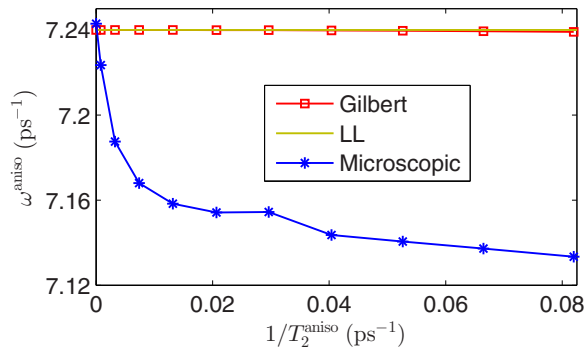


FIG. 18. (Color online) Precession frequency of the localized spin around the anisotropy field vs Bloch decay time $1/T_2^{\text{aniso}}$.

resulting dependence of the Gilbert parameter α_{aniso} on $1/T_2$ in both approaches is in qualitative accordance and exhibits two different regimes. In the low spin-flip regime, where $1/T_2$ is small in comparison to the p - d exchange interaction, a linear increase of α_{aniso} with $1/T_2$ is found, as is the case in our calculations with microscopic dephasing terms. If the relaxation rate is larger than the p - d dynamics, α_{aniso} decreases again. Due to the restriction (36) of the Boltzmann scattering integral to low spin-flip rates, the present Markovian calculations cannot be pushed into this regime.

Even though the anisotropy field \vec{H}_{aniso} is not coupled to the localized spin \vec{S} directly, both spins precess around the z direction with frequency ω_L^{aniso} . In analogy to Sec. VB, we study now the influence of the damping process on the precession of the localized spin around the anisotropy axis and compare it to the behavior of Landau-Lifshitz and Gilbert dynamics. Figure 18 reveals a similar behavior of the precession frequency as a function of the damping rate $1/T_2^{\text{aniso}}$ as in the isotropic case. The microscopic calculation predicts a distinct drop of the Larmor frequency ω_L^{aniso} for a range of dephasing rates where the precession frequency is unchanged according to the Gilbert and Landau-Lifshitz damping models. Although Gilbert damping eventually leads to a change in precession frequency for larger damping, this result shows a qualitative difference between the microscopic and the phenomenological calculations.

VII. CONCLUSION AND OUTLOOK

In this paper, we investigated a microscopic description of dephasing processes due to spin-orbit coupling and electron-

phonon scattering in a mean-field kinetic exchange model. We first analyzed how spin-dependent carrier dynamics can be described by Boltzmann scattering integrals, which leads to Elliott-Yafet-type relaxation processes. This is only possible for dephasing rates small compared to the Larmor frequency, see Eq. (36). The microscopic calculation always yielded Bloch times $2T_1 = T_2$ for low excitation angles as it should be due to the conservation of the absolute value of the magnetization. A small decrease of the effective precession frequency occurs with increasing damping rate, which is a fundamental difference to the Landau-Lifshitz description and exceeds the change predicted by the Gilbert equation in this regime.

We modeled two dephasing scenarios. First, a relaxation process between both spin subsystems was studied. Here, the different spins precess around the mean-field of the other system. In particular, for large excitation angles, we found a decrease of the magnetization during the precessional motion without heating and a slow remagnetization. This scenario is somewhat in between typical small angle relaxation, for which the modulus of the magnetization is constant and which is well described by Gilbert and Landau-Lifshitz damping, and collinear de/remagnetization dynamics. Also, we find important deviations from a pure Bloch-like behavior.

The second scenario deals with the relaxation of the magnetization toward a magnetic anisotropy field experienced by the itinerant carrier spins for small excitation angles. The resulting Gilbert parameter α_{aniso} is independent of the static anisotropy field. The relaxation of the localized moments occurs only indirectly as a carrier-mediated relaxation via their coupling to the time-dependent mean-field of the itinerant spin.

To draw a meaningful comparison with Landau-Lifshitz and Gilbert dynamics, we restricted ourselves throughout the entire paper to a regime where the electronic temperature is equal to the lattice temperature T_{ph} at all times. In general, our microscopic theory is also capable of modeling heat induced de- and remagnetization processes. We intend to compare microscopic simulations of hot electron dynamics in this model, including scattering processes between both types of spin, with phenomenological approaches such as the Landau-Lifshitz-Bloch (LLB) equation or the self-consistent Bloch equation (SCB) [43].

ACKNOWLEDGMENT

Svenja Vollmar is a recipient of funding through the Excellence Initiative (DFG/GSC 266).

- [1] L. Landau and E. Lifshitz, *Phys. Z. Sowjetunion* **8**, 153 (1935).
- [2] T. L. Gilbert, *IEEE Trans. Magn.* **40**, 3443 (2004).
- [3] D. L. Mills and R. Arias, *The damping of spin motions in ultrathin films: Is the Landau-Lifshitz-Gilbert phenomenology applicable?* Invited paper presented at the VII Latin American Workshop on Magnetism, Magnetic Materials and their Applications, Renaca, Chile, 2005.
- [4] D. A. Garanin, *Physica A* **172**, 470 (1991).

- [5] V. V. Andreev and V. I. Gerasimenko, *Sov. Phys. JETP* **35**, 846 (1959).
- [6] A. Brataas, Y. Tserkovnyak, and G. E. W. Bauer, *Phys. Rev. Lett.* **101**, 037207 (2008).
- [7] W. M. Saslow, *J. Appl. Phys.* **105**, 07D315 (2009).
- [8] N. Smith, *Phys. Rev. B* **78**, 216401 (2008).
- [9] M.-C. Hickey and J. S. Moodera, *Phys. Rev. Lett.* **102**, 137601 (2009).

- [10] S. Wienholdt, D. Hinzke, K. Carva, P. M. Oppeneer, and U. Nowak, *Phys. Rev. B* **88**, 020406(R) (2013).
- [11] U. Atxitia, O. Chubykalo-Fesenko, R. W. Chantrell, U. Nowak, and A. Rebei, *Phys. Rev. Lett.* **102**, 057203 (2009).
- [12] Z. Li and S. Zhang, *Phys. Rev. B* **69**, 134416 (2004).
- [13] O. Chubykalo-Fesenko, *Appl. Phys. Lett.* **91**, 232507 (2007).
- [14] D. A. Garanin, *Phys. Rev. B* **55**, 3050 (1997).
- [15] U. Atxitia and O. Chubykalo-Fesenko, *Phys. Rev. B* **84**, 144414 (2011).
- [16] I. Garate and A. MacDonald, *Phys. Rev. B* **79**, 064403 (2009).
- [17] K. Gilmore, I. Garate, A. H. MacDonald, and M. D. Stiles, *Phys. Rev. B* **84**, 224412 (2011).
- [18] J. Sinova, T. Jungwirth, X. Liu, Y. Sasaki, J. K. Furdyna, W. A. Atkinson, and A. H. MacDonald, *Phys. Rev. B* **69**, 085209 (2004).
- [19] Y. Tserkovnyak, G. A. Fiete, and B. I. Halperin, *Appl. Phys. Lett.* **84**, 5234 (2004).
- [20] K. Shen, G. Tatara, and M. W. Wu, *Phys. Rev. B* **81**, 193201 (2010).
- [21] K. Shen and M. W. Wu, *Phys. Rev. B* **85**, 075206 (2012).
- [22] L. Cywiński and L. J. Sham, *Phys. Rev. B* **76**, 045205 (2007).
- [23] T. Jungwirth, J. Sinova, J. Masek, J. Kucera, and A. H. MacDonald, *Rev. Mod. Phys.* **78**, 809 (2006).
- [24] T. Dietl, *Nat. Mater.* **9**, 965 (2010).
- [25] J. König, H.-H. Lin, and A. H. MacDonald, *Phys. Rev. Lett.* **84**, 5628 (2000).
- [26] J. König, T. Jungwirth, and A. H. MacDonald, *Phys. Rev. B* **64**, 184423 (2001).
- [27] A. Kirilyuk, A. V. Kimel, and T. Rasing, *Rev. Mod. Phys.* **82**, 2731 (2010).
- [28] S. Mangin, M. Gottwald, C.-H. Lambert, D. Steil, V. Uhlřř, L. Pang, M. Hehn, S. Alebrand, M. Cinchetti, G. Malinowski, Y. Fainman, M. Aeschlimann, and E. E. Fullerton, *Nat. Mater.* **13**, 286 (2014).
- [29] F. Bloch, *Phys. Rev.* **70**, 460 (1946).
- [30] N. Bloembergen, *Phys. Rev.* **78**, 572 (1950).
- [31] S. V. Vonsovskii, *Ferromagnetic Resonance* (Pergamon, Oxford, 1966).
- [32] D. D. Stancil and A. Prabhakar, *Spin Waves*, (Springer, New York, 2009).
- [33] D. Pines and C. Slichter, *Phys. Rev.* **100**, 1014 (1955).
- [34] C. Lü, J. L. Cheng, M. W. Wu, and I. C. da Cunha Lima, *Phys. Lett. A* **365**, 501 (2007).
- [35] B. Koopmans, J. J. M. Ruigrok, F. Dalla Longa, and W. J. M. de Jonge, *Phys. Rev. Lett.* **95**, 267207 (2005).
- [36] C. E. Patton, in *Magnetic Oxides*, edited by D. J. Craik (Wiley, London, 1975), Vol. 2.
- [37] M. Leontiadou, K. L. Litvinenko, A. M. Gilbertson, C. R. Pidgeon, W. R. Branford, L. F. Cohen, M. Fearn, T. Ashley, M. T. Emeny, B. N. Murdin, and S. K. Clowes, *J. Phys.: Condens. Matter* **23**, 035801 (2011).
- [38] H. Haug and S. W. Koch, *Quantum Theory of the Optical and Electronic Properties of Semiconductors*, 4th ed. (World Scientific, Singapore, 2003).
- [39] F. T. Vasko and O. E. Raichev, *Quantum Kinetic Theory and Applications* (Springer, New York, 2005).
- [40] K. Kaasbjerg, K. S. Thygesen, and A.-P. Jauho, *Phys. Rev. B* **87**, 235312 (2013).
- [41] H. C. Schneider, W. W. Chow, and S. W. Koch, *Phys. Rev. B* **70**, 235308 (2004).
- [42] J. Chovan and I. E. Perakis, *Phys. Rev. B* **77**, 085321 (2008).
- [43] L. Xu and S. Zhang, *J. Appl. Phys.* **113**, 163911 (2013).